Techniques Used in the F-14 Variable-Sweep Transition Flight Experiment

Bianca Trujillo Anderson,* Robert R. Meyer Jr.,* and Harry R. Chiles†
NASA Ames Research Center, Dryden Flight Research Facility, Edwards, California 93523

This article discusses and evaluates the test measurement techniques used to determine the laminar-to-turbulent boundary-layer transition location in the F-14 variable-sweep transition flight experiment (VSTFE). The main objective of the VSTFE was to determine the effects of wing sweep on the laminar-to-turbulent transition location at conditions representative of transport aircraft. Four methods were used to determine the transition location: 1) a hot-film anemometer system, 2) two boundary-layer rakes, 3) surface pitot tubes, and 4) liquid crystals for flow visualization. Of the four methods, the hot-film anemometer system was the most reliable indicator of transition.

Introduction

RECENTLY, an experiment was devised to determine the effects of wing sweep on natural boundary-layer transition location at flight conditions representative of transport aircraft. Performed on the swing-wing F-14 aircraft, the experiment, referred to as the F-14 variable sweep transition experiment (VSTFE),[1-4] was a joint effort between NASA Langley Research Center and NASA Ames-Dryden Flight Research Facility. The experiment involved using a foam and fiberglass technique to fit a smooth contoured surface to the wing of the aircraft. Two of these devices, called natural laminar-flow wing gloves, were flight tested. Glove 1 was flown in the first and second phases of the experiment, and glove 2, only in the second phase of the experiment. A hot-film anemometer system, boundary-layer rakes, surface pitot tubes, and liquid crystals were used to determine the transition location. The results of these four measurement techniques will be discussed and compared.

Test Aircraft

The F-14A aircraft (Fig. 1) was the carrier vehicle for the experiment. The F-14A has variable-wing-sweep capability, its flight envelope includes the Mach and Reynolds number range suitable for testing at conditions representative of modern intermediate size transport aircraft.

Both wing panels were modified by bonding an upper surface glove constructed of foam and fiberglass using the techniques described in Ref. 5. Each glove wrapped around the leading edge and extended back to the spoiler hinge line on the upper surface ($\approx$ 60% chord) and covered the majority of the span. These gloves provided a smooth surface (that is, $<$ 0.002 in. amplitude/2 in.), as well as space to install instrumentation, plumbing, and wiring.

Glove 1, a cleanup of the basic F-14A wing, was installed on the left-wing panel. The basic F-14 airfoil shape (a modified NASA 6 series) was used because it could provide pressure distributions with very favorable pressure gradients near Mach 0.800. Glove 2, installed on the right-wing panel, involved major modifications to the F-14 airfoil shape, but it provided a much broader Mach number range and a variety of pressure distributions, for which transition data could be obtained. With the gloves installed, the maximum wing sweep was restricted to 35 deg.

Instrumentation

The F-14A aircraft was instrumented with a standard NACA noseboom[6,7] to measure total and static pressure, angle of attack, and angle of sideslip. The cockpit was instrumented with an uplink display system, described in Ref. 8, that was used to assist the pilot in obtaining accurate flight conditions. The glove instrumentation (Fig. 2) consisted of surface static pressure orifices, boundary-layer rakes, surface pitot tubes (glove 1 only), and hot-film anemometers.

Surface Static Pressure Orifices

The surface static pressures were used to examine the glove pressure distribution and to determine the amount of favorable pressure gradient obtained for each test point. Each orifice row was oriented streamwise to the flow for a wing sweep of 20 deg, as shown in Fig. 2.

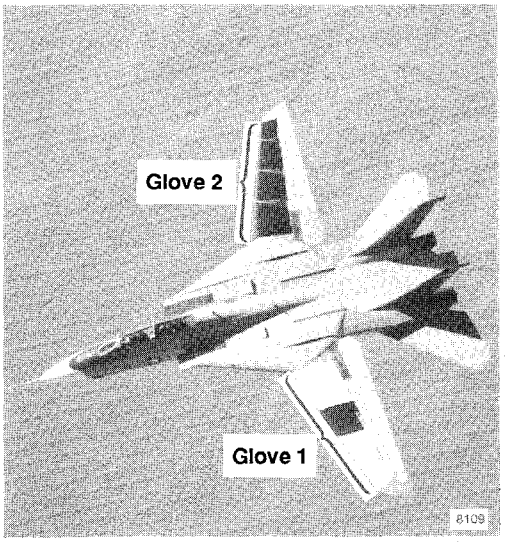

Fig. 1 F-14A aircraft with gloves 1 and 2.

Presented as Paper 88-2110 at the AIAA 4th Flight Test Conference, San Diego, CA, May 18–20, 1988; received July 31, 1989; revision received Sept. 1, 1990; accepted for publication Sept. 4, 1990.

*Aerospace Engineer, Aerodynamics Branch, Research Engineering Division. Member AIAA.

†Aerospace Engineer, Flight Instrumentation Branch, Research Engineering Division.

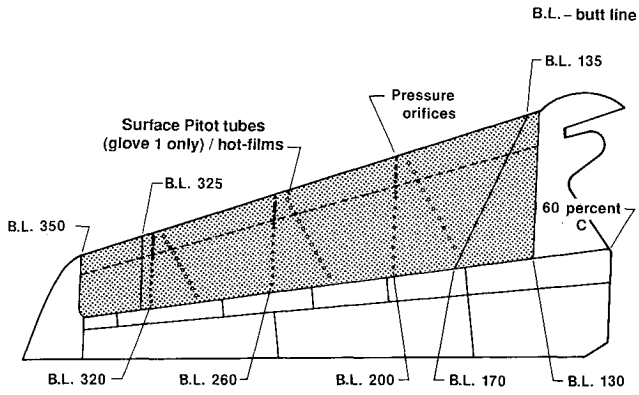

Fig. 2 Glove planform and general instrumentation layout.

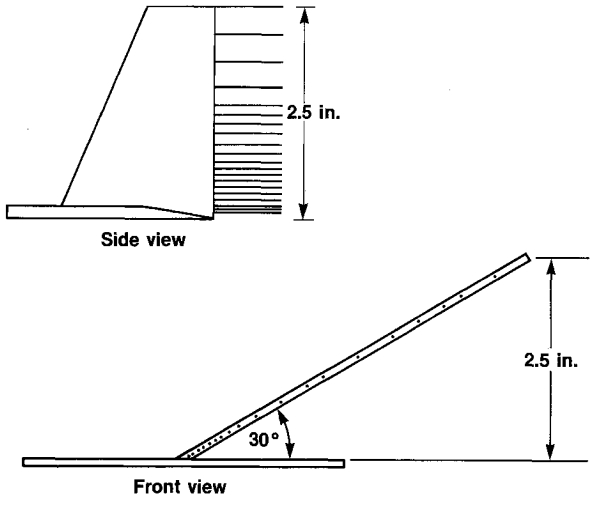

Fig. 3 Diagram of boundary-layer rake.

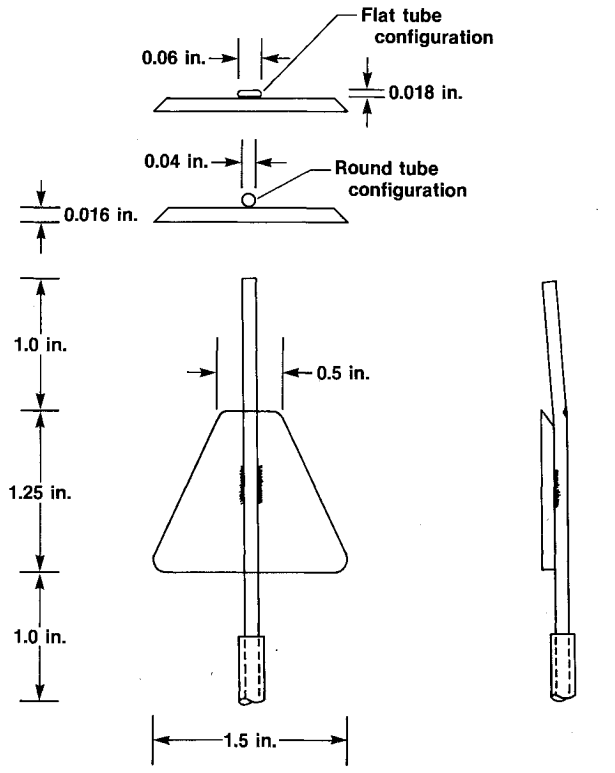

Fig. 4 Schematic of surface pitot tube.

Boundary-Layer Rakes

Each boundary-layer rake consisted of 20 pressure probes. These rake probes were mounted along a 4-in. plate that was skewed 30 deg to a plane normal to the glove surface, as shown in Fig. 3. Each rake was oriented streamwise to the flow for a wing sweep of 20 deg.

Surface Pitot Tubes

The surface pitot tubes (Fig. 4) were mounted flush to the glove surface. For the first half of the glove 1 flights, the tubes were left rounded. For the second half of the flights, the tubes were flattened into an oval shape.

Three rows of surface pitot tubes were mounted on glove 1, with a maximum of 11 tubes/row. As illustrated in Fig. 2, each row was located along a line oriented at a 30-deg angle to each orifice row. This was to alleviate interferences between each tube and the hot films, which were also oriented along this line. Each individual tube, however, was oriented to be streamwise to the flow for a wing sweep of 20 deg. The surface pitot tubes were not installed on glove 2.

Hot-Film Sensors

Five hot-film sensors were operational for glove 1, and 15 were operational for glove 2. The location of the operational hot-film sensors for both gloves varied from flight to flight. The glove 1 hot-film system used constant-temperature hot-film anemometers.[9-11] Based on the desire for more measurements to reduce the number of flights for acquiring data, a newly designed temperature-compensated hot-film anemometer system was used for glove 2.[12]

The hot-film sensors, as shown in Fig. 2, were mounted along a line oriented at a 30-deg angle to the leading edge of the glove to minimize any flow disturbance from one sensor affecting another sensor (flow is turbulent after each sensor). The typical hot-film-sensor spacing was 10% chord; however, some data were obtained with the hot-film sensors spaced every 5% chord. The hot-film sensors for glove 1 (Fig. 5a) were oriented streamwise to the flow for a wing sweep angle of 20 deg. Because the hot-film sensors used for the glove 2 system (Fig. 5b) were expected to be more sensitive to flow angle, the hot-film sensor orientation was tilted 5 deg, making them streamwise to the flow at a wing sweep of 25 deg. Both types of hot films were able to detect transition to the maximum sweep angle of 35 deg.

In addition to the normal ac (dynamic) output, the temperature-compensated hot-film anemometer used on glove 2 also provided a dc (steady-state) output. The frequency response of the hot-film sensors was 150 kHz, as determined by the manufacturer. The tape recorder used, however, had a frequency response of 10 kHz, thereby limiting the recorded hot-film data to a frequency response of 10 kHz.

Test Conditions

Boundary-layer transition data were obtained at the flight conditions listed in Table 1. Transition data at 15 deg of sweep were obtained by using a sideslip maneuver, because the minimum wing sweep available was 20 deg. The aircraft would fly the test point with ±5 deg of sideslip to obtain an equivalent wing sweep of 15 deg for the right and left gloves, respectively.

The maneuvers used to obtain data were steady-state trim points, windup turns, or pushovers. Using these three maneuvers, data at angles of attack other than trim were acquired for constant Mach, sweep, and altitude.

Results

The four techniques used to determine the transition location are discussed in the following sections. The transition data shown represent typical examples of the data obtained.

Hot-Film Data

The results obtained from the hot-film anemometers were based on ac and dc signals. An example of a typical dynamic signal is shown in Fig. 6a. Dynamic signals originating in areas of laminar flow were of lower amplitude or "quieter" than those originating in areas of turbulent flow. Additional indicators were high-amplitude spikes in the output signal; high-amplitude spikes in a direction of positive voltage indicated a mostly laminar signal with occasional turbulent bursts, whereas high-amplitude spikes in a negative direction indicated a mostly turbulent signal with occasional laminar bursts. These two types of signals were indicators of the beginning and ending of the transition region. Maximum occurrence of these high-amplitude spikes was at peak transition, the region where the flow is most unstable. The transition location was defined as the location where peak transition occurred. In many cases, the hot-film sensors were not spaced close enough to always define the transition region. In cases where one sensor was laminar and the next was fully turbulent, transition was defined at the midpoint. The real-time ground station dynamic signal plots were generally acceptable for determining transition location; however, in some cases the postflight high-frequency response plots were needed for clarification.

An example of a typical steady-state signal is shown in Fig. 6b. Steady-state signals originating in areas of laminar flow were of a lower level than those originating in areas of turbulent flow. In general, instantaneous changes in the steady-state level indicated peak transition. The instantaneous changes or oscillations in the steady-state signal level occurred because the steady-state signal had a frequency response of 500 Hz. This allowed some of the dynamic signal to be picked up by the steady-state signal. The real-time ground station steady-state-signal time histories were usually acceptable; however, in areas at or nearing peak transition, the postflight dynamic signal plots were sometimes necessary to aid in interpreting the steady-state output data.

Figures 7 present examples of anomalies encountered in the steady-state signal. A comparison is made between two steady-

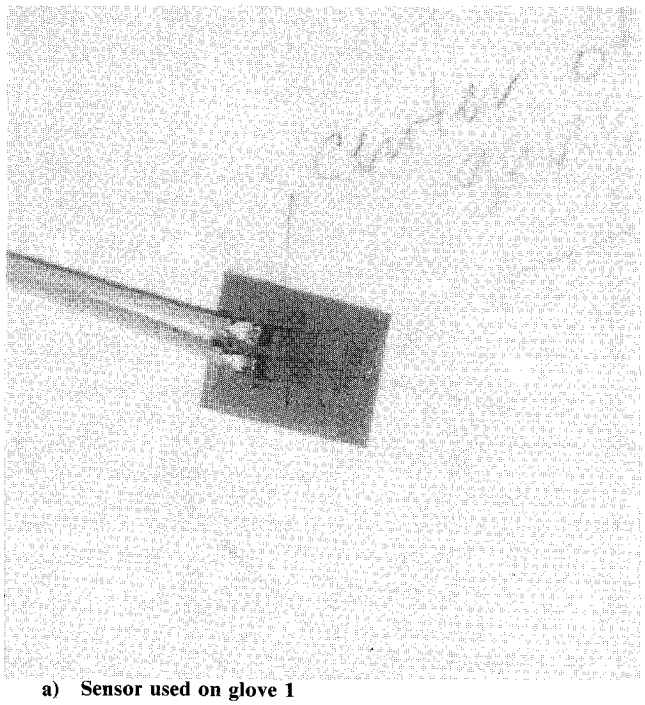

a) Sensor used on glove 1

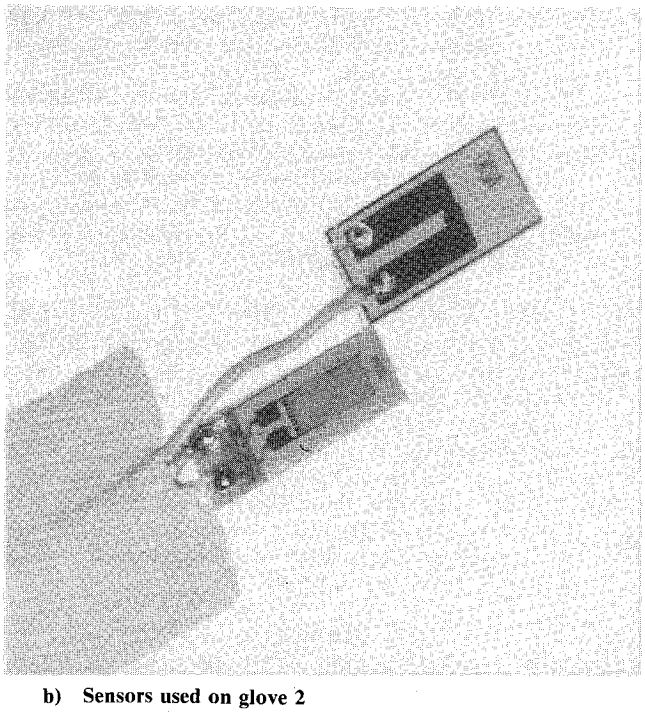

b) Sensors used on glove 2

Fig. 5 Hot-film sensors.

Table 1 Test conditions[a]

Sweep, deg	Sideslip, deg
20	0,5,-5
25	0
30	0
35	0

[a]Mach: 0.600, 0.650, 0.700, 0.750, 0.800, 0.825; altitude: 10,000, 20,000, 25,000, 30,000, 35,000 ft; angle of attack: 0–5 deg.

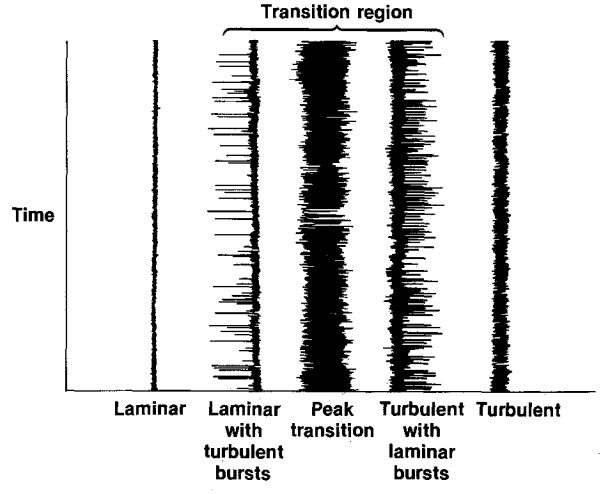

a) Dynamic, ac, hot-film output signals

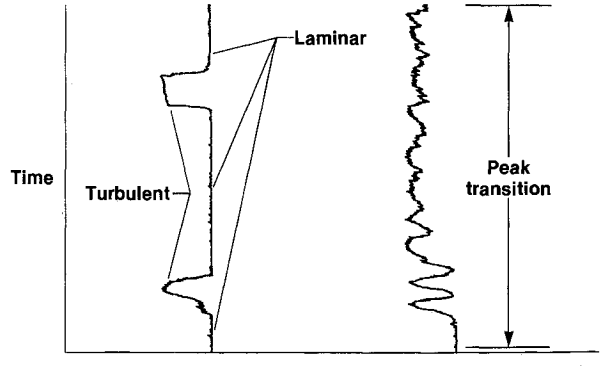

b) Steady-state output signal

Fig. 6 Typical hot-film output signals.

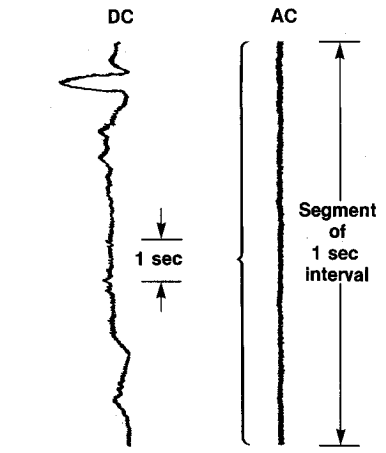

a) Laminar dc and ac signals

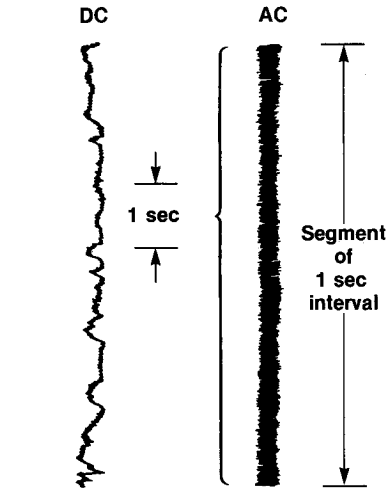

b) Laminar dc signal and turbulent ac signal

Fig. 7 Hot-film signal comparisons.

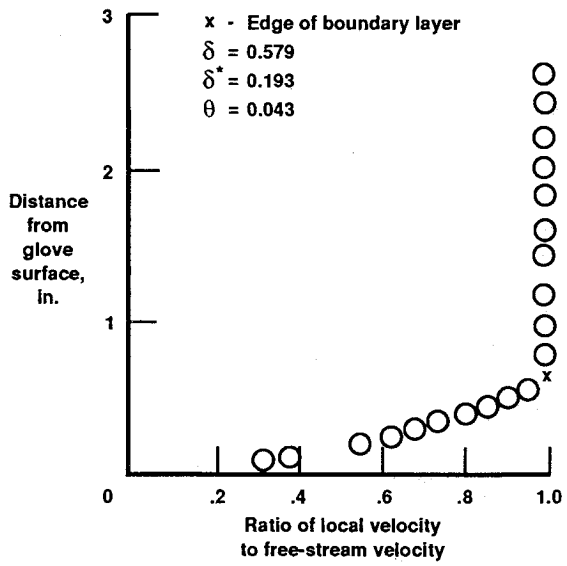

Fig. 8 Typical boundary-layer profile.

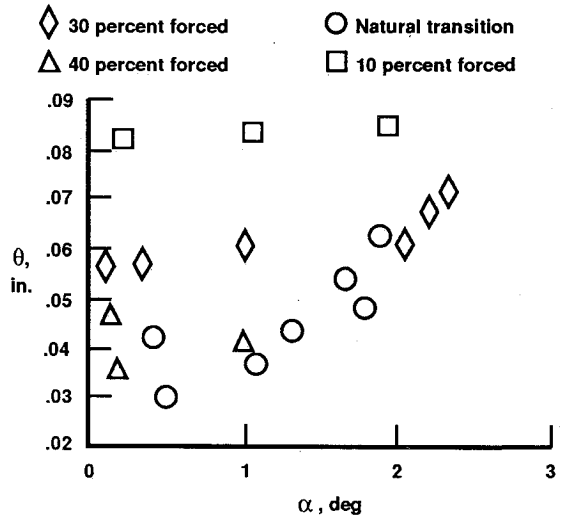

Fig. 9 Boundary-layer-rake transition data.

state and dynamic signals at the same time intervals. The steady-state signal is at a laminar level for each case. The corresponding dynamic signal is laminar for the first case (Fig. 7a) and fully turbulent for the second case (Fig. 7b). With these types of discrepancies existing in the steady-state signal, in areas at or near the transition location, the dynamic signal was easier to interpret.

The degee to which transition can be determined is limited only by the distance between the hot-film sensors and experience in interpreting the hot-film output signal. For the VSTFE, the hot-film spacing was generally 10% chord (c) for glove 1 and most of the glove 2 data; however, some glove 2 data were obtained with a hot-film sensor spacing of 5% c for better resolution.

Based on the spacing of the hot-film sensors, the five types of dynamic hot-film outputs, and the experience gained in interpreting data for 2700 test points, the accuracy of the transition data obtained from the hot-films is estimated at $\pm 2.5\%$ c for gloves 1 and 2. The transition data obtained did not define the entire transition region (that is, the first occurrence of a turbulent burst to the last occurrence of a laminar burst). Defining the transition region would require closer spacing of the hot-film sensors.

Boundary-Layer Data

The boundary-layer-rake data provided a velocity profile of the boundary-layer and skin-friction-related parameters such as boundary-layer height δ, displacement thickness δ^*, and momentum thickness Θ.[13] A typical boundary-layer profile with the corresponding calculated values of δ, δ^*, and Θ is shown in Fig. 8. The skin-friction parameters were available only from the boundary-layer-rake data.

Determining the transition location from the boundary-layer-rake data required a calibration of the boundary-layer thickness as a function of chordwise transition location. Calibration of the rake data was achieved by forcing the boundary layer to transition at various chord locations, using a ⅛-in.-wide transition strip of Carborundum grit. The grit was sized using the method described in Ref. 14. When the flow is forced to transition at known locations, δ, δ^*, and Θ can be obtained as a function of the chordwise transition location and the angle of attack.

When the rake calibration was completed, the location of natural transition for the glove could be determined. An example of a calibration plot with naturally transitioning data is shown in Fig. 9. Figure 9 is a plot of momentum thickness as a function of angle of attack for data obtained at the same flight condition as the data shown in Fig. 8. Each line indicates values of Θ obtained when the boundary layer was forced to transition using the transition strips at the indicated chordwise locations, 10, 30, and 40% c. The Θ value for the velocity profile in Fig. 8 is plotted in Fig. 9, along with the rest of the natural transitioning data at the same flight condition, and is represented by a solid circle. Based on Fig. 9, natural transition occurs aft of 40% c and begins to move forward as the angle of attack α increases.

A comparison of the transition results from the boundary-layer-rake data and the hot-film data is presented in Fig. 10. The boundary-layer-rake data agreed to within $\pm 5\%$ c with the hot-film data. For the majority of the cases, the transition location indicated by the boundary-layer-rake data agreed with the transition location indicated by the hot films. It is interesting to note that the boundary-layer-rake data generally indicated transition just aft of the hot-film data. This is consistent with the definition of transition location for both the hot films and the boundary-layer rakes. For the hot films, transition location was picked at peak transition location, and for the rakes, the calibration of transition location was based on fully turbulent flow.

Surface Pitot Tube Data

The third method used to determine the transition location was the surface pitot tubes. The local total pressure value measured from the surface pitot tube was subtracted from the total pressure measured from the aircraft noseboom and denoted as ΔP. This ΔP was plotted as a function of the ratio of chordwise distance from leading-edge to local chord length (x/c), as shown in Fig. 11. Interpretation of the surface pitot tube data was based on previous experiments using pitot tubes to determine the transition location.[15-17] Using this method, if a pitot tube is outside the boundary-layer, ΔP will be essentially zero, equal to the aircraft total pressure, because the pitot tube is in freestream flow. If the flow is in the boundary layer, ΔP is not equal to zero. If the flow is laminar, or transition occurs at the leading edge, ΔP increases uniformly in the direction of the flow and may level off (Fig. 12). If the flow transitions at some point aft of the leading edge, there will be a local decrease in ΔP at that location, and then ΔP will continue to increase uniformly and may level off (Fig. 11).

Figures 13a and 13b are typical cases where transition could easily be determined from the surface pitot tube data. In both of these cases, the transition location is indicated by the local decrease in ΔP. Figures 14a and 14b are typical cases where transition location could not be easily determined from the surface pitot tube data. These figures have more than one area where ΔP decreases locally.

Figures 15a and 15b show transition location determined from the surface pitot tube data compared to transition loca-

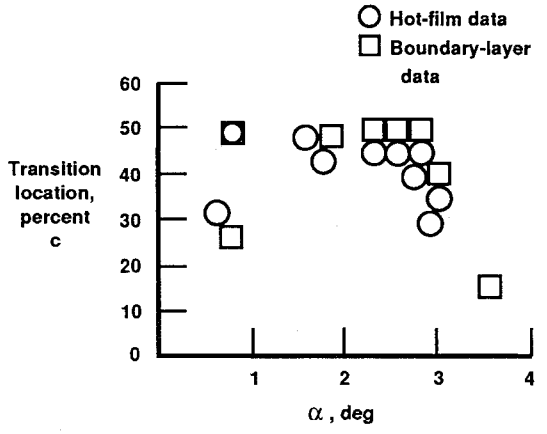

Fig. 10 Comparison of hot-film and boundary-layer data.

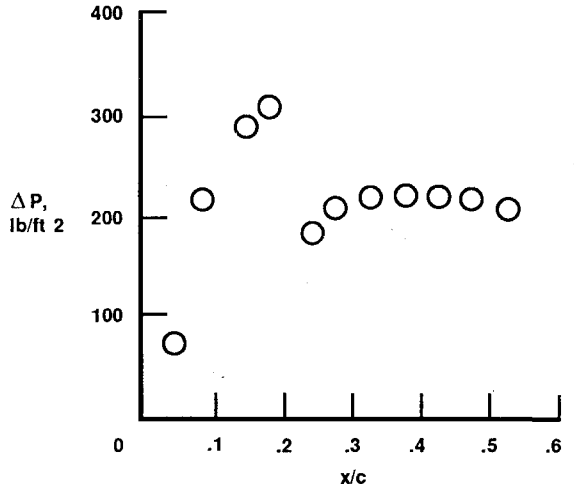

Fig. 11 Typical surface pitot tube data.

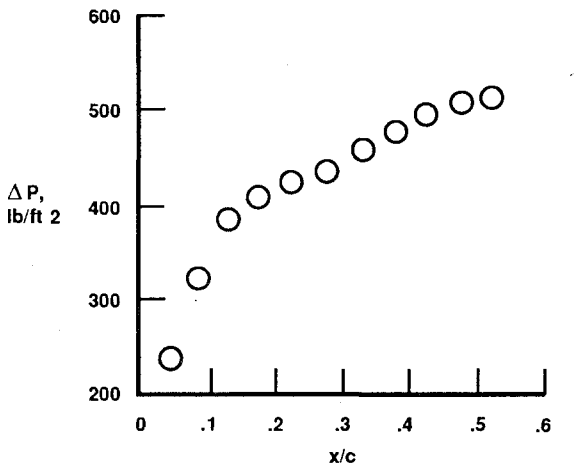

Fig. 12 Laminar or fully turbulent surface pitot tube data.

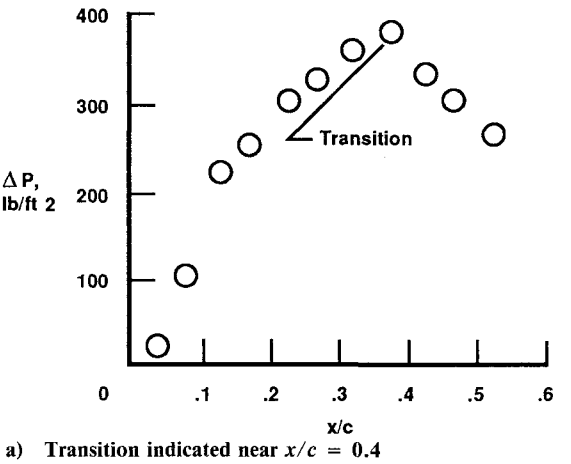

a) Transition indicated near $x/c = 0.4$

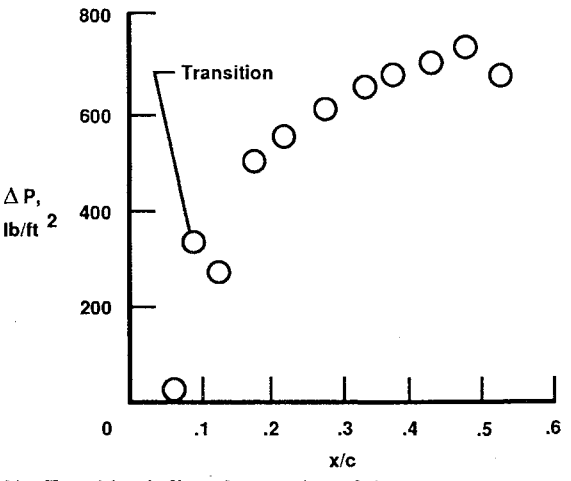

b) Transition indicated near $x/c = 0.1$

Fig. 13 Typical surface pitot tube transition data.

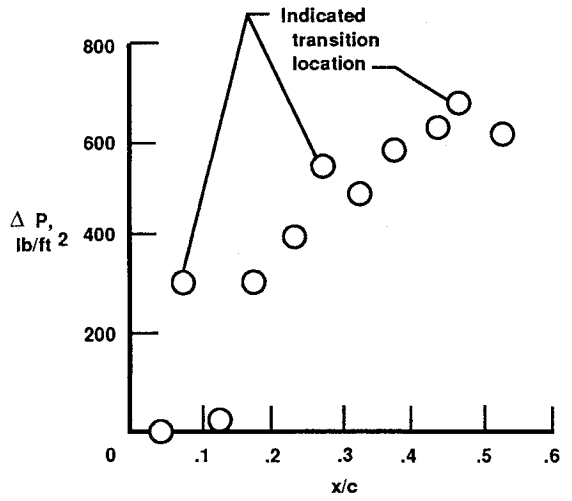

a) Transition indicated in two directions

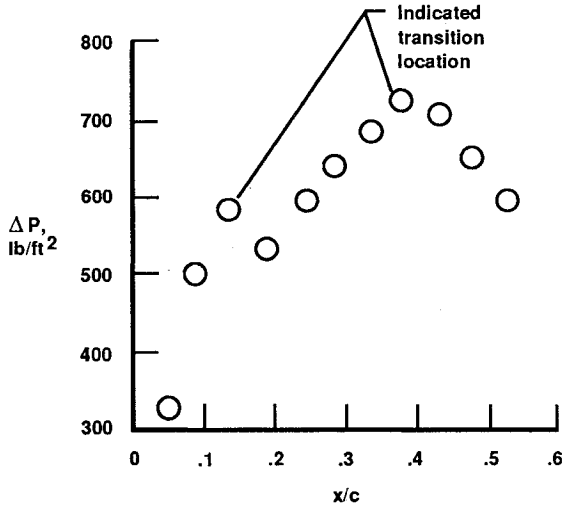

b) Transition indicated in three directions

Fig. 14 Surface pitot tube data indicating more than one transition location.

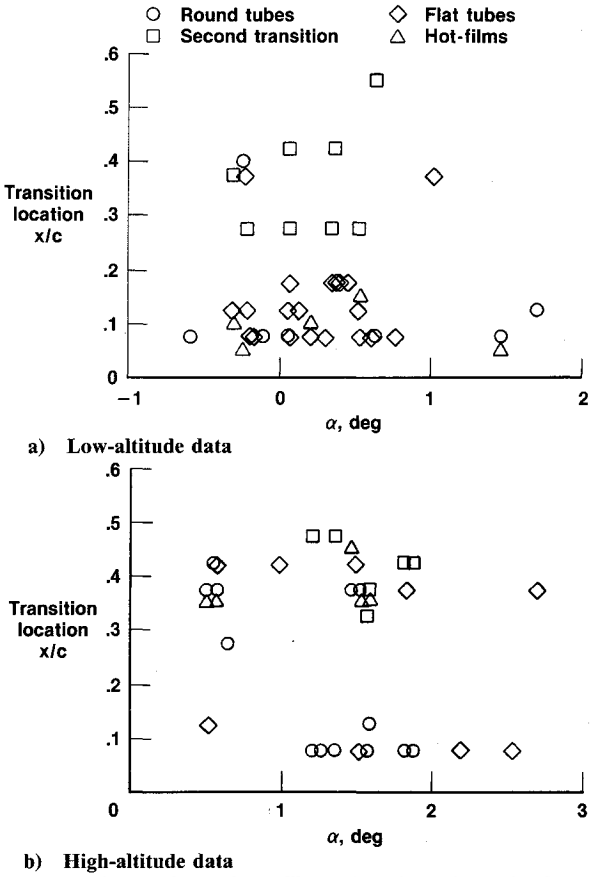

a) Low-altitude data

b) High-altitude data

Fig. 15 Comparison of hot-film and surface pitot tube data.

tion determined from the hot films. For the cases where two local decreases in ΔP were observed in the surface pitot tube data, two apparent transition locations were plotted. The second apparent transition location is indicated by the dotted square symbols. Figures 15 also contain surface pitot tube data with tubes in round and flattened configurations and distinguished by squares and triangles, respectively.

A large amount of scatter in the surface pitot tube data is evident in Figs. 15. In general, there is no difference between the transition location indicated by the round tube configuration and the flat tube transition. The hot-film data agree with some of the pitot tube data however. For case a (Fig. 15a), the first transition location indicated by the surface pitot tubes agreed with the hot-film data. For case b (Fig. 15b), the second transition location indicated by the surface pitot tubes agreed with the hot-film data.

The general trend of the surface pitot tube data is that at higher dynamic pressures the first transition location indicated by the surface pitot tubes agrees with the hot-film data; at higher altitudes, the hot-film data agree with the second transition location indicated by the surface pitot tube data.

A preliminary look at the trends and anomalies in the surface pitot tube data shows that some of the decreases in ΔP correspond to sudden changes in the pressure distribution. However, there were many anomalies of this type noted in the surface pitot tube data that have not been accounted for. The surface pitot tubes may have picked up local adverse changes in total pressure that did not, in all cases, cause transition and may not have occurred uniformly across the span of the glove. These adverse changes in pressure may not have been detected by the hot films, because the two sets of instrumentation were not at the same x/c or span locations. Laminar flow is capable of withstanding a small level of adverse pressure gradients in some cases and, therefore, a small level of increased local total pressure may not always be the result of laminar-to-turbulent transition.

Because of the many anomalies, the criteria used to determine transition from the surface pitot tube data were not always successful. Although the surface pitot method used in this experiment was not entirely successful, previous experiments have used surface pitot tubes successfully to indicate transition. Past experiments,[15-17] however, have used a higher probe density or a traversing probe, producing higher resolution data. More surface pitot tubes would have increased the resolution of the ΔP as a function of x/c curves. However, with the glove 1 instrumentation configuration, adding more surface pitot tubes was not feasible.

Flow Visualization Data

The fourth method used to determine the transition location was flow visualization using pressure-sensitive liquid crystals. This technique is similar to that used in Ref. 18. The middle test section of glove 1 and all of glove 2 were painted black to provide contrast for the liquid crystals. The liquid crystal mixture was applied to the glove surface before takeoff.

Both still and video photography of the liquid crystal patterns were obtained. Figures 16 show examples of liquid crystal patterns. Transition is indicated by a change in color in the liquid crystal pattern. The colors themselves are not important because they change with viewing angle as well as with the transition location.

Figures 17 present a comparison of liquid crystal and hot-film transition data obtained at the same time intervals. Data are included for glove 1 and glove 2. These figures show that the transition location indicated by the liquid crystal pattern

agreed to within ±5% c with the hot-film indication of transition location at the same time interval. Based on the good agreement between the liquid crystal patterns and the hot-film data for the same time interval, the hot-film sensors were used to indicate transition locations with liquid crystals on the surface for test points where photographs were not taken.

Figures 18 show a comparison of transition data obtained with and without liquid crystals on the glove surface. The transition location is plotted as a function of angle of attack. At the lower altitude, all of the transition data obtained with liquid crystals on the glove surface fall below the transition data obtained without the liquid crystals on the glove surface.

In the high-altitude plot of Fig. 18, there is only a 5% c variation in the transition location for all of the data obtained. The transition location does not appear to be affected by the presence of the liquid crystals.

The use of liquid crystals for flow visualization produced mixed results. The advantage of the liquid crystal patterns is that transition is obtained globally, as opposed to several discrete locations. The flow visualization method is relatively easy to use and requires only a camera for documentation.

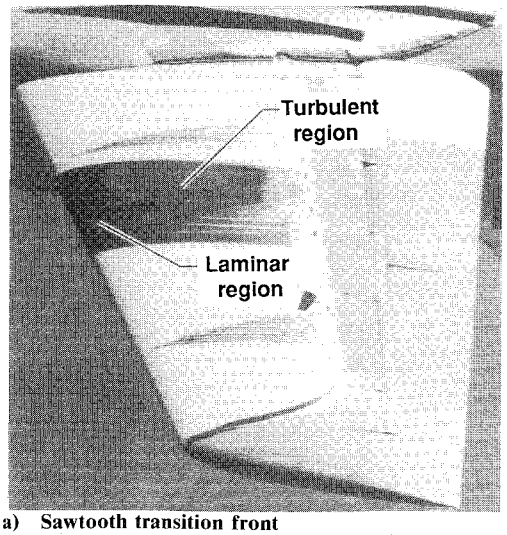

a) Sawtooth transition front

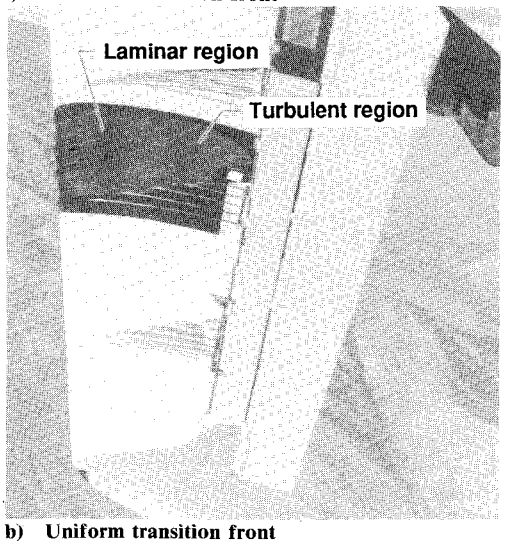

b) Uniform transition front

Fig. 16 Examples of liquid crystal patterns.

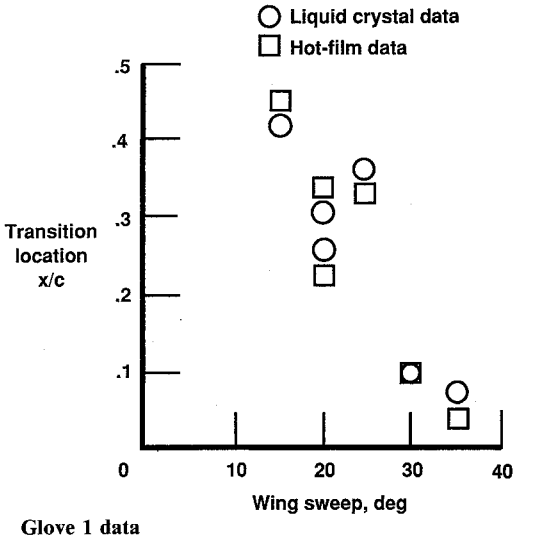

a) Glove 1 data

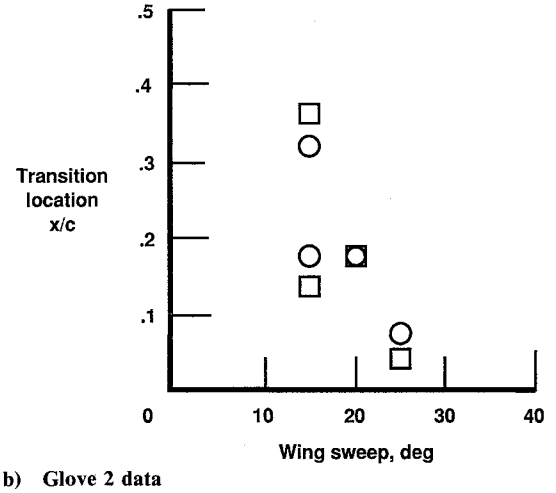

b) Glove 2 data

Fig. 17 Comparison of hot-film and liquid crystal data.

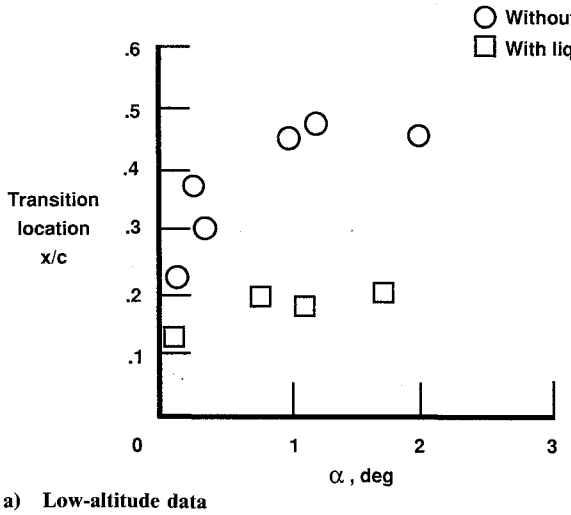

a) Low-altitude data

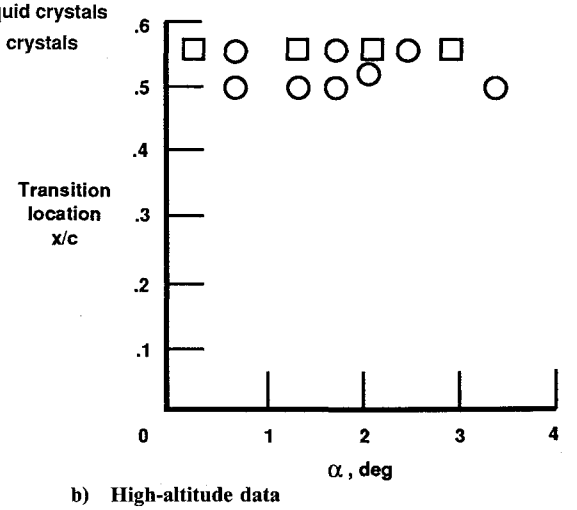

b) High-altitude data

Fig. 18 Comparison of transition data with and without liquid crystals on the glove surface.

Several drawbacks were noted, however. First, insects and dust tend to adhere to the glove surface in greater amounts with the presence of the liquid crystals. The insect impacts and dust particles produce discontinuities that can cause localized transition. The localized turbulent region appears as a wedge in the liquid crystal pattern, such as those found in Fig. 16a.

Second, an uneven thickness in the liquid crystal coat can cause changes of the color in the liquid crystal pattern, interfering with the interpretation of the pattern. Therefore, care must be taken in applying the liquid crystal coat evenly. Third, at lower altitudes (that is, $< 25{,}000$ ft) or higher unit Reynolds numbers, the presence of the liquid crystals was observed to affect the transition location, as illustrated in Figs. 18.

Comparing the four techniques, the hot-film data were the easiest to interpret. Transition was indicated in real time by the hot films, whereas the data obtained from all the other methods had to be analyzed postflight. In addition, the boundary-layer data needed to be calibrated, which required several flights. The boundary-layer rakes produced repeatable data, however, and were used as a secondary method. The surface pitot tube data did not consistently indicate transition, although they have been successfully used in previous experiments. The liquid crystals were the easiest to use. At altitudes above 25,000 ft, the transition location indicated by the liquid crystal patterns agreed with the hot-film and boundary-layer data. However, the liquid crystals caused transition to occur further forward at altitudes below 25,000 ft.

Conclusions

Presented in this article were the results of using four techniques to determine the laminar-to-turbulent boundary-layer transition location in the variable-sweep transition flight experiment (VSTFE). The four techniques were 1) a hot-film anemometer system, 2) boundary-layer rakes, 3) surface pitot tubes, and 4) liquid crystals for flow visualization.

The hot-film anemometer system provided the most accurate indication of the transition location and was the primary method used in the VSTFE to determine the transition location. Transition was determined from both dynamic and steady-state hot-film signals in real time. Of the two types of hot-film output signals, the dynamic signal was a better indicator of the transition location when the transition occurred at or near the hot-film sensor. The accuracy of the data obtained with the hot-film anemometer system used in the VSTFE was approximately $\pm 2.5\%$ chord (c). Closer spacing of the hot films would be required, however, to define the entire transition region.

The boundary-layer rakes served as a good secondary indicator of the transition location. The boundary-layer-rake data agreed to within $\pm 5\%$ c with the hot-film data. One advantage of the boundary-layer-rake method is that it provided skin-friction-related parameters in addition to an indication of the transition location.

The surface pitot tube method used in the VSTFE did not consistently indicate transition. There were many cases where more than one apparent transition location was indicated by the surface pitot tube data. The first transition location indicated by the surface pitot tube data generally agreed with the hot-film data for the lower altitude cases, whereas the second transition location indicated by the surface pitot tube data agreed with the hot-film data for the higher altitude cases. Some of the decreases in the difference between aircraft total pressure and local total pressure, measured from the surface pitot tubes (ΔP) did correspond to sudden changes in the pressure distributions; however, not all of the anomalies can be accounted for. One improvement in the surface pitot tube configuration would have been closer spacing of the surface pitot tubes. Unfortunately, this was not a feasible alternative for the VSTFE.

The liquid crystals were very useful as a tool for flow visualization. The liquid crystal method provides a global view of the transition location. This method is easiest to use because no instrumentation is required, only a camera. However, there were certain drawbacks. With the presence of the liquid crystals on the glove surface, an increase in the amount of insect impacts was noted. Color changes occurred in the liquid crystal patterns as a result of uneven thicknesses in the liquid crystal coats. Last, the transition location had a tendency to move forward at lower altitudes or higher unit Reynolds numbers with the presence of the liquid crystals on the glove surface.

Overall, the test techniques used were successful in indicating the transition location and can be useful for boundary-layer and fluid dynamics-related experiments.

References

[1]Meyer, R. R., Trujillo, B. M., and Bartlett, D. W., "F-14 VSTFE and Results of the Cleanup Flight Test Program," *Natural Laminar Flow and Laminar-Flow Control,* NASA CP-2487, Pt. 3, March 1987, pp. 819–844.

[2]Waggoner, E. G., Campbell, R. L., Phillips, P. S., and Hallissy, J. B., "Design and Test of an NLF Wing Glove for the Variable-Sweep Transition Flight Experiment," *Natural Laminar Flow and Laminar-Flow Control,* NASA CP-2487, Pt. 3, March 1987, pp. 753–776.

[3]Rozendaal, R. A., "Variable Sweep Transition Flight Experiment (VSTFE)—Stability Code Development and Clean-Up Glove Data Analysis," *Natural Laminar Flow and Laminar-Flow Control,* NASA CP-2487, Pt. 3, March 1987, pp. 845–859.

[4]Rozendaal, R. A., "Variable Sweep Transition Flight Experiment (VSTFE)—Parametric Pressure Distribution Boundary Layer Stability Study and Wing Glove Design Task," NASA CR-3992, June 1986.

[5]Bohn-Meyer, M., "Constructing 'Gloved' Wings for Aerodynamic Studies," AIAA Paper 88-2109, May 1988; also NASA TM-100440, 1988.

[6]Gracy, W., Letko, W., and Russell, W. R., "Wind-Tunnel Investigation of a Number of Total-Pressure Tubes at High Angles of Attack Subsonic Speeds," NACA TN-2331, April 1951.

[7]Sakamoto, G. M., "Aerodynamic Characteristics of a Vane Flow Angularity Sensor System Capable of Measuring Flightpath Accelerations for the Mach Number Range from 0.4 to 2.54," NASA TN D-8242, May 1976.

[8]Meyer, R. R., Jr., and Schneider, E. T., "Real-Time Pilot Guidance System for Improved Flight Test Maneuvers," AIAA Paper 83-2747, Nov. 1983.

[9]Chiles, H. R., and Johnson, J. B., "Development of a Temperature-Compensated Hot-Film Anemometer System for Boundary-Layer Transition Detection on High-Performance Aircraft," NASA TM-86732, Aug. 1985.

[10]Collier, F. S., Johnson, J. B., Rose, O. J., and Miller, D. S., "Supersonic Boundary-Layer Transition on the LaRC F-106 and the DFRF F-15 Aircraft," *Natural Laminar Flow and Laminar-Flow Control,* NASA CP-2847, Pt. 3, March 1987, pp. 997–1024.

[11]Johnson, J. B., "Preliminary In-Flight Boundary Layer Transition Measurements on a 45-Degree Swept Wing at Mach Numbers Between 0.9 and 1.8," NASA TM-100412, March 1988.

[12]Chiles, H. R., "The Design and Use of a Temperature-Compensated Hot-Film Anemometer System for Boundary-Layer Flow Transition Detection on Supersonic Aircraft," NASA TM-100421, May 1988.

[13]Saltzman, E. J., and Fisher, D. F., "Some Turbulent Boundary-Layer Measurements Obtained from the Forebody of an Airplane at Mach Numbers up to 1.72," NASA TN D-5838, June 1970.

[14]Braslow, A. L., and Knox, E. C., "Simplified Method for Determination of Critical Height of Distributed Roughness Particles for Boundary-Layer Transition at Mach Numbers from 0 to 5," NACA TN-4363, Sept. 1958.

[15]Fisher, D. F., and Fischer, M. C., "Development Flight Tests of JetStar LFC Leading-Edge Flight Test Experiment," NASA CP-2487, Pt. 1, March 1987, pp. 117–140.

[16]Fisher, D. F., and Dougherty, N. S., Jr., "In-Flight Transition Measurement on a 10° Cone at Mach Numbers from 0.5 to 2.0," NASA TP-1971, June 1982.

[17]Matting, F. W., Chapman, D. R., Nyholm, J. R., and Thomas, A. G., "Turbulent Skin Friction at High Mach Numbers and Reynolds Numbers in Air and Helium," NASA TR R-82, 1961.

[18]Holmes, B. J., Gall, P. D., Croom, C. C., Manuel, G. S., and Kelliher, W. C., "A New Method for Laminar Boundary Layer Transition Visualization in Flight—Color Changes in Liquid Crystal Coatings," NASA TM-87666, Jan. 1986.